ACS OMEGA

http://pubs.acs.org/journal/acsodf

Article

Synthesis of Biogenic Silver Nanocatalyst and their Antibacterial and Organic Pollutants Reduction Ability

Muhammad Riaz, Uzma Sharafat, Nafeesa Zahid, Muhammad Ismail,* Jeongwon Park,* Bashir Ahmad, Neelum Rashid, Muhammad Fahim, Muhammad Imran, and Aisha Tabassum

Cite This: *ACS Omega* 2022, 7, 14723−14734

Read Online

ACCESS | Metrics & More | Article Recommendations

ABSTRACT: Plant-mediated nanoparticles are gaining popularity due to biologically active secondary metabolites that aid in green synthesis. This study describes a simple, environmentally friendly, dependable, and cost-effective production of silver nanoparticles utilizing *Cucumis sativus* and *Aloe vera* aqueous leaf extracts. The aqueous leaf extracts of *Cucumis sativus* and *Aloe vera*, which worked as a reducing and capping agent, were used to biosynthesize silver nanoparticles (AgNPs). The formation of surface plasmon resonance peaks at 403 and 405 nm corresponds to the formation of colloidal Ag nanoparticles. Similarly, the Bragg reflection peaks in X-ray diffraction patterns observed at 2θ values of 38.01°, 43.98°, 64.24°, and 77.12° representing the planes of [111], [200], [220], and [311] correspond to the face-centered cubic crystal structure of silver nanoparticles. Fourier transform infrared spectroscopy confirms that bioactive chemicals are responsible for the capping of biogenic silver nanoparticles. The size, structure, and morphology of AgNPs with diameters ranging from 8 to 15 nm were examined using transmission electron microscopy. Water contamination by azo dyes and nitrophenols is becoming a more significant threat every day. The catalytic breakdown of organic azo dye methyl orange (MO) and the conversion of *para*-nitrophenol (PNP) into *para*-aminophenol using sodium borohydride was evaluated using the prepared biogenic nanoparticles. Our nanoparticles showed excellent reduction ability against PNP and MO with rate constants of 1.51 × 10^{-3} and 6.03 × $10^{-4}s^{-1}$, respectively. The antibacterial activity of the nanomaterials was also tested against four bacteria: *Staphylococcus aureus*, *Klebsiella pneumoniae*, *Enterobacter*, and *Streptococcus pneumoniae*. These biogenic AgNPs displayed effective catalytic and antibacterial characteristics by reducing MO and PNP and decreasing bacterial growth.

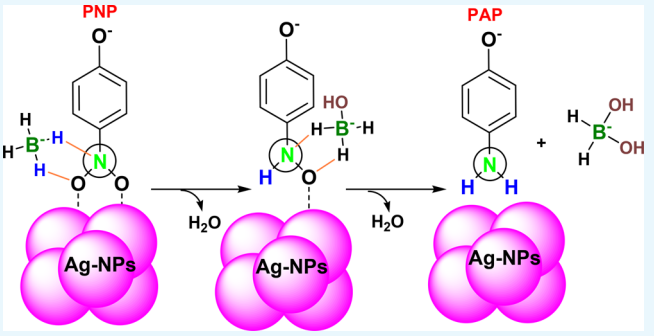

1. INTRODUCTION

Nanomaterials research has exploded in popularity in recent years, affecting nearly every science and industry because of the irreplaceable qualities that massive materials lack. Three key characteristics control and influence the behavior of nanomaterials: shape, size, and crystallinity.[1,2] Noble metal nanoparticles, such as Ag or Au, have been discovered to have unique features among diverse biosynthesized metal nanoparticles, including optical,[3] catalytic,[4] and antibacterial properties.[5] The first step in investigating the many properties of these nanoparticles is to synthesize them. Chemical and physical methods of producing nanoparticles have been interchangeable for decades. Therefore, biological processes were also investigated for the same reason: they provide a straightforward, low-cost, and environmentally beneficial option.[1] The use of various fungi,[6] bacteria,[7] and plant[8] extracts to produce silver nanoparticles (AgNPs) is a well-studied topic these days. Further, extracts from common plants have been utilized to generate Ag nanoparticles from silver salts, but they have not been widely employed. Moreover, on the one hand, plant extracts are often used as reducing agents, responsible for the reduction and stability of nanoparticles when they interact with metal ions. On the other hand, Riaz et al. described that plant extracts could be quite effective because they contain significant reducing and capping agents.[9]

Because of electrostatic interactions between silver ions and proteins in plant material extract, the bioreduction of Ag was considered to involve capturing Ag^+ ions on the protein surface. Proteins reduce the Ag^+ ions, resulting in a change in secondary structure and the formation of silver nuclei. Silver nuclei are formed by further reducing Ag^+ ions and their build-

Received: December 29, 2021
Accepted: April 1, 2022
Published: April 19, 2022

up at the nucleus, resulting in the production of AgNPs.[10] The fundamental mechanism driving the plant-mediated synthesis of AgNPs, according to our findings, is a plant-assisted reduction caused by phytochemicals found in *Cucumis sativus* and *Aloe vera* fruit peel extract. The primary phytochemicals in *Aloe vera* include vitamins (A (beta-carotene), C, and E), enzymes (aliiase, amylase, alkaline phosphatase, bradykinase, carboxypeptidase, cellulase, catalase, lipase, and peroxidase), sugars (monosaccharides glucose and fructose) and polysaccharides (polymannose/glucomannans), fatty acids (plant steroids, campesterol, cholesterol, β-sisosterol, and lupeol), and anthraquinones (phenolic compounds).[11] Organic acids, quinones, and flavones, water-soluble phytochemicals, are responsible for rapidly reducing silver ions in the reaction mixture. According to reports, xerophytes include anthraquinone and emodin, which undergo tautomerization and result in the creation of AgNPs.[12] In most situations, the reducing agent from the plant extract also serves as a capping and stabilizing agent, removing the need for external capping and stabilizing chemicals.[13] It has been discovered that the type of plant extract employed as a reducing agent affects the reduction of silver ions.[14]

Water contamination is currently one of the most important environmental issues, owing to the presence of organic color molecules.[15,16] Among the various nitroaromatic chemicals, nitrophenols are the most common contaminant of industrial effluents. Aqueous nitrophenol effluents are common industrial wastes produced during various organic products, including pharmaceuticals, insecticides, herbicides, plasticizers, dyes, and explosives. Nitrophenols are extremely difficult to biodegrade, posing a threat to the environment, and are carcinogenic to humans.[17−19] Therefore, the Environmental Protection Agency of the United States (U.S. EPA) has designated nitrophenol and its derivatives as priority contaminants, proposing that their concentration in natural water bodies be kept to no more than 10 mg/mL. Nitrophenols irritate the eyes and cause necrosis of the skin. It also harms the liver, kidneys, and muscles. One gram of nitrophenols has been reported to be fatal to an adult.[20] Carcinogenic amines are produced in aquatic bodies due to reducing azo and nitro chemicals.[21] Because of its complex aromatic chemical structure and xenobiotic properties, methyl orange (MO) dye is nonbiodegradable. MO is an organic sulfur salt azo dye that is widely used in the food, textiles, paper, pulp, and leather industries as an indicator and reagent. MO dye and its metabolites are widely leaking into the aquatic environment, posing a health danger.[22−24] The use of metal nanoparticles for the catalytic degradation of organic dyes and nitroaromatic compounds is an essential method for converting hazardous chemicals into environmentally beneficial chemicals. Because of its outstanding catalytic activity and eco-friendly characteristics, this approach is widely utilized for the remediation of recalcitrant contaminants.[25] On the one hand, for the photodegradation of organic contaminants, semiconductor-based materials such as CeO_2, Fe_2O_3/ZnO, and WO_3/Ce_2S_3 nanotubes have recently been employed.[26,27] Metal oxides, on the other hand, have a disadvantage in that they do not absorb visible light.

This paper describes the biological generation of silver nanoparticles by reducing Ag^+ ions with *Cucumis sativus* peel extract and *Aloe vera* leaf extract. The catalytic activity of the colloidal particles was tested using established techniques such as MO dye degradation in the presence of $NaBH_4$ as a reducing agent and catalytic hydrogenation of *para*-nitrophenol (PNP) to *para*-aminophenol (PAP). Further to employ beneficial constituents, specifically phytochemicals present in both plant extracts, prepared nanoparticles have been used for antimicrobial activity. Antibacterial activities of these nanoparticles were tested against four bacteria: *Staphylococcus aureus*, *Klebsiella pneumoniae*, *Enterobacter*, and *Streptococcus pneumoniae*.

2. EXPERIMENTAL SECTION

2.1. Materials. *Aloe vera* and *Cucumis sativus* were purchased from a local market to make the peel extract. Merck provided the $AgNO_3$ (Merck KGaA, purity: 99.0%), MO (Merck), $NaBH_4$ (Merck KGaA, purity: 98.0%), and PNP (Sigma-Aldrich, ≥99%) needed for this project. The University of Ottawa Science Shop was used to purchase four bacterial strains.

2.2. Preparation of Silver Nanoparticles. *Aloe vera* and *Cucumis sativus* were chosen for the biosynthesis of AgNPs because of their cost-effectiveness, availability, and medicinal properties. Biosynthesis was performed in the manner previously described[28] with minor modifications. A grinder was used to smash 50 g of *Aloe vera* and cucumber peel extracts, which had been cleaned and crushed in 500 mL of distilled water. It was then filtered and centrifuged at 5000 rpm for 5 min, yielding a clear soup containing both extracts.

The silver nitrate solution was made by dissolving 3.38 g of $AgNO_3$ in 1000 mL of distilled water to make a 20 mM $AgNO_3$ stock solution. 100 mL of 20 mM $AgNO_3$ solution was mixed with each extract, drop by drop, until the medium was half diluted to reduce the number of Ag^+ ions in the silver nitrate solution. The reacting mixture was agitated at ambient temperature before a noticeable alteration in the color of the solution, as exhibited in Figure 1. After the reaction was completed, the mixture was centrifuged for 30 min at 10 000 rpm to separate the nanoparticles from the remaining constituents. The nanoparticle precipitate was redispersed in deionized water (10 mL) in the centrifuge tube. This suspension was centrifuged for 15 min at 5000 rpm in ethanol to remove the biomass residue altogether. The pellet of nanoparticles in the centrifuge tube was dried in a vacuum drier, yielding a dry powder of biogenic AgNPs. These dry AgNPs were used for various characterizations discussed further below.

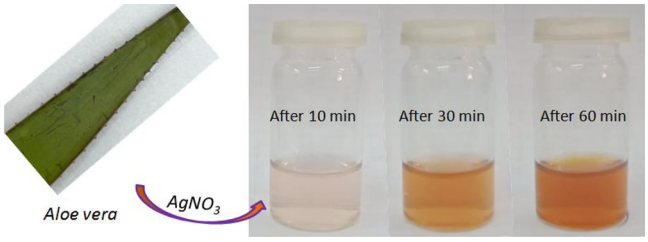

Figure 1. Pictorial presentation of the synthesis of *Aloe vera*-mediated biogenic AgNPs (photograph courtesy of Muhammad Riaz. Copyright 2022).

2.3. Characterization of Silver Nanoparticles. The absorption spectra of the prepared nanoparticles mixture were recorded by a PerkinElmer UV−visible spectrometer at regular intervals by scanning the reacting mixture from 200 to 800 nm. The Rigaku Ultima-III X-ray diffractometer was used to

https://doi.org/10.1021/acsomega.1c07365
ACS Omega 2022, 7, 14723−14734

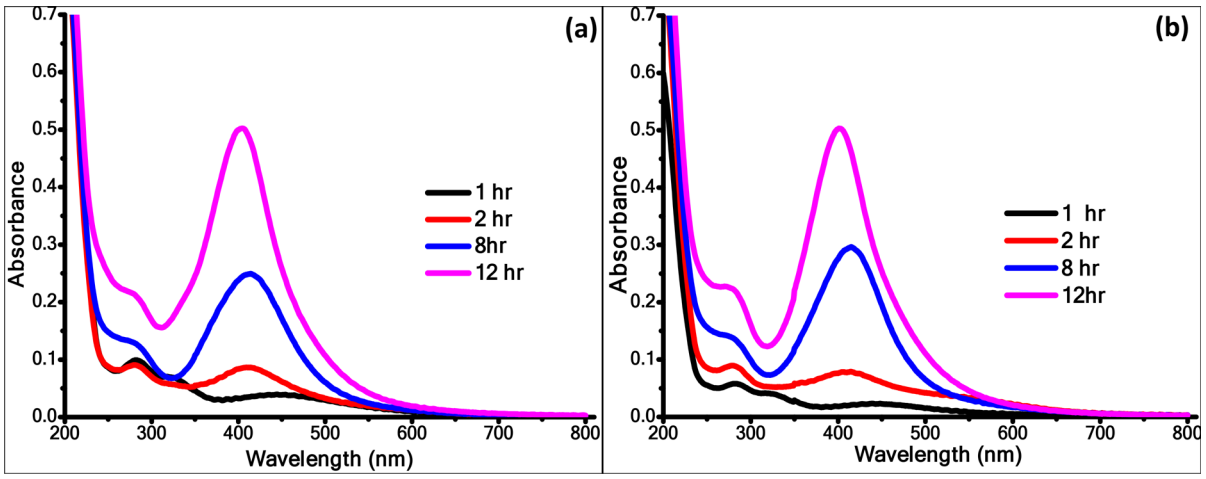

Figure 2. UV−Visible spectra for the continuous growth of AgNPs. (a) *C. sativus*-mediated AgNPs and (b) *Aloe vera*-mediated AgNPs. Experiments were performed at room temperature. Measurements were taken at 1, 2, 8, and 12 h intervals.

analyze the crystalline nature of dried biogenic Ag nanoparticles. An IR-Prestige (Shimadzu) Fourier transform infrared (FTIR) spectrometer was used to record the FTIR spectra of biogenic Ag nanoparticles. For the transmission electron microscopy (TEM) analysis, high-resolution JEOL-2010 TEM (operating voltage is 200 kV) was used. The zeta potential of AgNPs was recorded using water as a solvent and Zetasizer Nano S90 (Malvern) at room temperature.

2.4. Catalytic Reduction Reactions. AgNPs were used to catalyze the reduction of the dyes MO and PNP. A 1 mM aqueous solution was prepared to catalyze PNP in DI water. The reaction vessel was a UV quartz cuvette. After a quartz cuvette was put in, the UV−visible spectra of 3 mL of PNP solution were obtained. Then added 0.5 mL of freshly prepared 0.5 M concentration $NaBH_4$ solution. The solution color changed from bright yellow to dark yellow. In the quartz cuvette containing the solution mixture, 10 mg of Ag catalyst was added. Reduction began when the nanoparticles were added to the cuvette, and spectra were recorded using a UV−visible spectrometer between 200 and 800 nm (PerkinElmer). For MO dye, 0.04 mM concentration was used, following the same experimental procedure.

The catalytic proficiency of the catalysts was determined from UV−visible spectra with the following equation

$$\text{percent degradation} = 100 - \left(\frac{A_t \times 100}{A_0}\right) \quad (1)$$

where A_0 is the initial absorbance (at λ_{max} 404 nm for PNP and 462 nm for MO), and A_t is the absorbance at different time intervals (t).

2.5. Antibacterial Activity Study. The antibacterial activity of AgNPs was analyzed using the well diffusion method against two Gram-positive bacteria, *S. aureus* and *S. pneumoniae*, and two Gram-negative bacteria, *K. pneumonia* and *Enterobacter*. The culture strains were kept on appropriate media composed of nutrient agar and regular agar powder. By comparing the results, clarithromycin was used as a positive control. After that, the bacteria were grown in an incubator at 37 °C for 24 h. Following the incubation period, the antibacterial activity was determined by monitoring and measuring the inhibition zone around the wells.

3. RESULTS AND DISCUSSION

3.1. Synthesis of Nanoparticles. Aqueous solutions of *Cucumis sativus* (*C. sativus*) and *Aloe vera* extract were used to reduce silver nitrate into AgNPs. The color change primarily proved the reduction of silver ions from light green to dark red.[29] The formation of AgNPs began when the addition of plant extracts started with silver nitrate solution, which changed the color of the reaction from light greenish to yellowish after 10 min. Organic biomolecules of *Aloe vera* and *C. sativus* extracts are thought to be effective in the reduction as well as capping nanoparticles. After an hour of extract addition (Figure 1), implying the origination of colloidal Ag nanoparticles in the mixture. After 8 h of incubation, the color changed to a dark brown as the reaction time increased.

3.2. UV−Vis Spectroscopy. A UV−visible spectrometer was employed to scan the mixture at regular intervals to monitor the formation of silver nanoparticles over time. The peak absorbance was found at 403 nm in the case of *C. sativus*-mediated AgNPs, as presented in Figure 2a, and at 405 nm in the case of *Aloe vera*-mediated AgNPs, as depicted in Figure 2b. The formation of surface plasmon resonance (SPR) peaks of AgNPs corresponds to colloidal Ag nanoparticles.[30] Figure 2a,b shows UV−visible spectra acquired at different time intervals (1, 2, 8, and 12 h). The peak absorbance rose with reaction time, and the variance is depicted in the figures. The peak absorbance increased linearly to 12 h of incubation, indicating that more colloidal particles were produced in the reacting media. The formation rate saturates after 12 h of incubation, indicating that the reaction is complete. The absorbance value at 12 h was most excellent, indicating that a substantial number of nanoparticles formed over time.

3.3. XRD Analysis. After the centrifugation and drying of the colloidal silver solution, the XRD analysis of *C. sativus*- and *Aloe vera*-mediated AgNPs were performed. The XRD pattern of prepared AgNPs is identical to that reported in our previous paper.[31] All the perceived peaks specify metallic silver crystallite. In the XRD pattern of both *C. sativus*- and *Aloe vera*-mediated AgNPs, the Bragg reflection peaks were observed at a 2θ value of 38.01°, 43.98°, 64.24°, 77.12°, and 81.4° representing the planes of [111], [200], [220], [311], and [222] (Figure 3). The crystalline face-centered cubic structures of AgNPs match these planes.[32,33] All the peaks in the XRD pattern of AgNPs can be indexed as a standard Ag

https://doi.org/10.1021/acsomega.1c07365
ACS Omega 2022, 7, 14723−14734

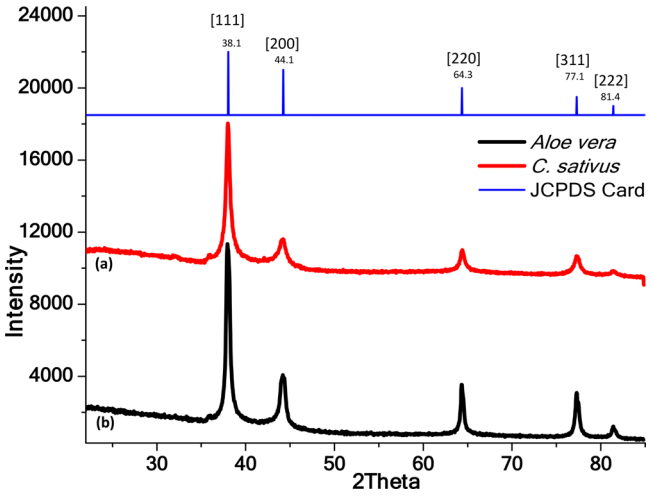

Figure 3. XRD patterns of (a) *C. sativus*-mediated AgNPs and (b) *Aloe vera*-mediated AgNPs.

crystal (JCPDS No. 4-0783).[33,34] XRD patterns of *C. sativus* and *Aloe vera* revealed no extra peak, confirming the pure crystalline nature of prepared AgNPs.

The Scherrer equation was used to compute the average crystallite size of biogenic AgNPs.

$$L = \frac{k\lambda}{\beta_{1/2} \cos\theta} \quad (2)$$

Here, λ (1.5418 Å) is the wavelength of X-rays, θ is the Bragg angle, $\beta_{1/2}$ is full width at half-maximum (fwhm) at the 2θ scale, and k is a constant equal to unity.

The average crystallite size of *C. sativus*-mediated AgNPs was 12−20 nm (mean size of ∼15 ± 2.5 nm), ably supported by TEM images. Similarly, the average crystallite size of *Aloe vera*-mediated AgNPs was 15−24 nm (mean size of ∼19 ± 3.8 nm). The lack of other peaks in the XRD data implies that the biosynthesized Ag nanoparticles are pure and crystalline.

3.4. TEM Analysis. The surface morphology and the average size of the prepared biogenic silver NPs were determined using high-resolution transmission electron microscopy (Figures 4 and 5). In the literature, it has been demonstrated that the shape and size of nanoparticles have a considerable impact on their optical and electrical properties. According to TEM histograms, the synthesized silver NPs are spherical and monodispersed, with some having a highly truncated triangular shape. According to TEM images, *C. sativus*-mediated silver nanoparticles are generally spherical in shape (Figure 4). Figure 4 shows the particle size and a histogram of *C. sativus*-mediated AgNPs, which have an average diameter of 14.29−14.7 nm. Similarly, TEM images (shown in Figure 5) indicate that the silver nanoparticles produced by *Aloe vera* are spherical. Figure 5 depicts the particle size and histogram of biogenic Ag NPs mediated by *Aloe vera*, with an average diameter of 8.4−11 nm.

3.5. EDS and Zeta Potential. The elemental composition of our synthesized AgNPs was analyzed using an energy-dispersive X-ray spectrum (EDX). Furthermore, the EDX spectroscopy provides both quantitative and qualitative details about the elements that were present in the NPs. The analysis was performed at the University of Ottawa. The elemental analysis of AgNPs was determined by putting the fabricated nanoparticles on carbon-coated thin films. The EDX spectrum of our synthesized AgNPs exhibited strong signals in the silver region for both samples, and an absorption peak was observed at 3 keV (Figures 6a,b). On the one hand, the peak in this region at 3 keV is due to the SPR of Ag, indicating the successful formation of AgNPs.[35] On the other hand, some other signals, including carbon, oxygen, chlorine, and silicon, were also detected in both synthesized AgNPs. The presence of these elements could have acted as capping agents of plant extract attached to the surface of synthesized AgNPs.[36]

Zeta potential is the scale of electrostatic interaction in nanoparticles and can be used to predict the stability of the dispersion system. The zeta potential of AgNPs was recorded using water as solvent and Zetasizer Nano S90 (Malvern) at room temperature. Zeta potential is one of the important indicators to speculate on the stability of metallic NPs. According to previous studies, nanoparticles having values of zeta potential less than −25 mV or more than +25 mV exhibit a high degree of stability. On the one hand, because of interparticle attractions, dispersions with a low zeta potential value will ultimately coalesce. The zeta potential of nanoparticles, on the other hand, is highly influenced by the pH and electrolyte content of the dispersion.[37] In the absence of an electrolyte, the zeta potential of dispersed AgNPs in deionized water was −10.6 and −7.29 mV, as presented in Figure 6c. The zeta potential value of our *Aloe vera*-mediated AgNPs was −10.6 mV, and this comparatively negative zeta potential value is an origin of the exceptional stability of the silver colloids by the electrostatic repulsion. Carboxylate moieties are found in anionic polysaccharides like pectin, which is often found in *Aloe vera* extract, and are a likely source of negative zeta potential. Because some of the phytochemicals used are also amphiphilic, green-produced AgNPs might have a high degree of stability even if their zeta potentials were not in the above-mentioned range.[38] These negative values of zeta potential can be attributed to the presence of the negatively charged polyphenolic species, which capped the surface of nanoparticles.[39] For both samples, the magnitude of the zeta potential of *Aloe vera*-mediated Ag nanoparticles was found to be higher than that of *S. sativus*-mediated AgNPs indicating the level of stability of the AgNPs prepared by *Aloe vera* extract.

3.6. FTIR Spectroscopy. The identification of stabilizing and reducing agents was performed using an FTIR analysis of prepared AgNPs. FTIR spectroscopy is essential for detecting the organic functional groups in plant extracts, which are responsible for metal ion reduction and stability. Figure 6d shows the dried Ag nanoparticles' recorded FTIR spectrum (absorbance mode). There are six different peaks in the whole range of the recorded spectrum. The C−H bending of alkanes and the C═O stretching vibration of amides is responsible for the bands at 1260 and 1625 cm^{-1}, respectively.[40,41] The band at 801 cm^{-1} could represent the stretching of C−N bonds in amines, and the band between 2946 and 3219 cm^{-1} represents the stretching of O−H bonds in aromatic compounds (such as phenol).[42] At 1240 and 1533 cm^{-1}, the remaining two bands correspond to hydrocarbon C−O and C−H bond stretching and bending, respectively.[43] According to this investigation, the bioactive functional compounds found in *C. sativus* and *Aloe vera*, fruit extracts, such as phenols and amines, may reduce Ag ions and stabilize colloidal particles during the interaction.

3.7. Catalytic Reduction of Methyl Orange Dye. The textile industry's discharge of dye sewage into the aquatic environment is the primary source of water contamination. Methyl orange is a toxic wastewater pollutant that can cause

https://doi.org/10.1021/acsomega.1c07365
ACS Omega 2022, 7, 14723−14734

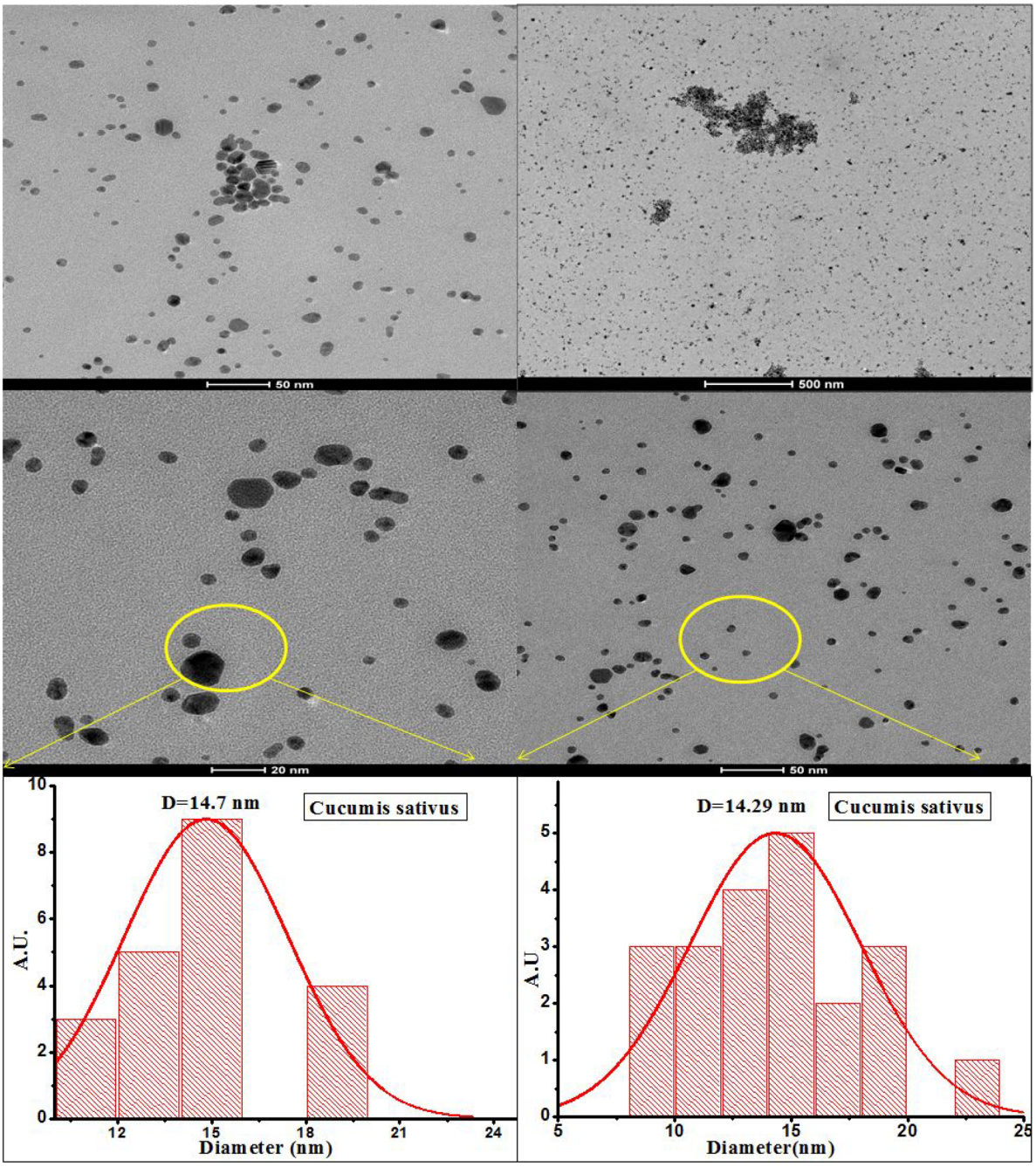

Figure 4. TEM images and particle distribution histogram of *C. sativus*-mediated AgNPs.

environmental impact. MO is commonly used as a laboratory indicator in the textile industry. The presence of the azo group and its low biodegradability make MO a severe environmental hazard.[44,45] As a result, the treatment of MO is a top priority. In the absence of a sufficient catalyst, reducing MO by sodium borohydride is kinetically inefficient but thermodynamically favorable. The peak intensity of MO at 462 nm has been reported to remain constant for longer time in the absence of a catalyst.[46]

For reduction, 3 mL of MO and 0.5 mL of $NaBH_4$ solutions were mixed in a quartz cuvette. An aqueous MO dye shows a significant absorption at 462 nm in the visible region and a smaller peak at 281 nm in the UV region. No changes in peak intensities occurred even after 20 min and were constant without AgNPs addition. After 5 mg of dry AgNPs was introduced, the drop in λ_{max} at 281 and 462 nm began. The UV−visible absorption spectra of the mixture were constantly collected at intervals of 1 min, as shown in Figure 7a. The peak intensity at 462 nm continuously decreased over time, as shown in Figure 7a, although the peak intensity at 282 nm marginally drifted to 252 nm with an increase in absorption. The drop in intensity at 462 nm with the progressive disappearance with AgNPs insertion was caused by the commencement of MO degradation. In the presence of a AgNPs catalyst, sodium borohydride reduced a molecule of MO dye at the azo site and thus formed smaller amino compounds. As a result, the $-NH_2$ group molecule produced during the reduction reaction of MO dye was ascribed to the new peak appearance at 252 nm with an increase in intensity.[47] It has been already reported that AgNPs minimize MO dye at

https://doi.org/10.1021/acsomega.1c07365
ACS Omega 2022, 7, 14723−14734

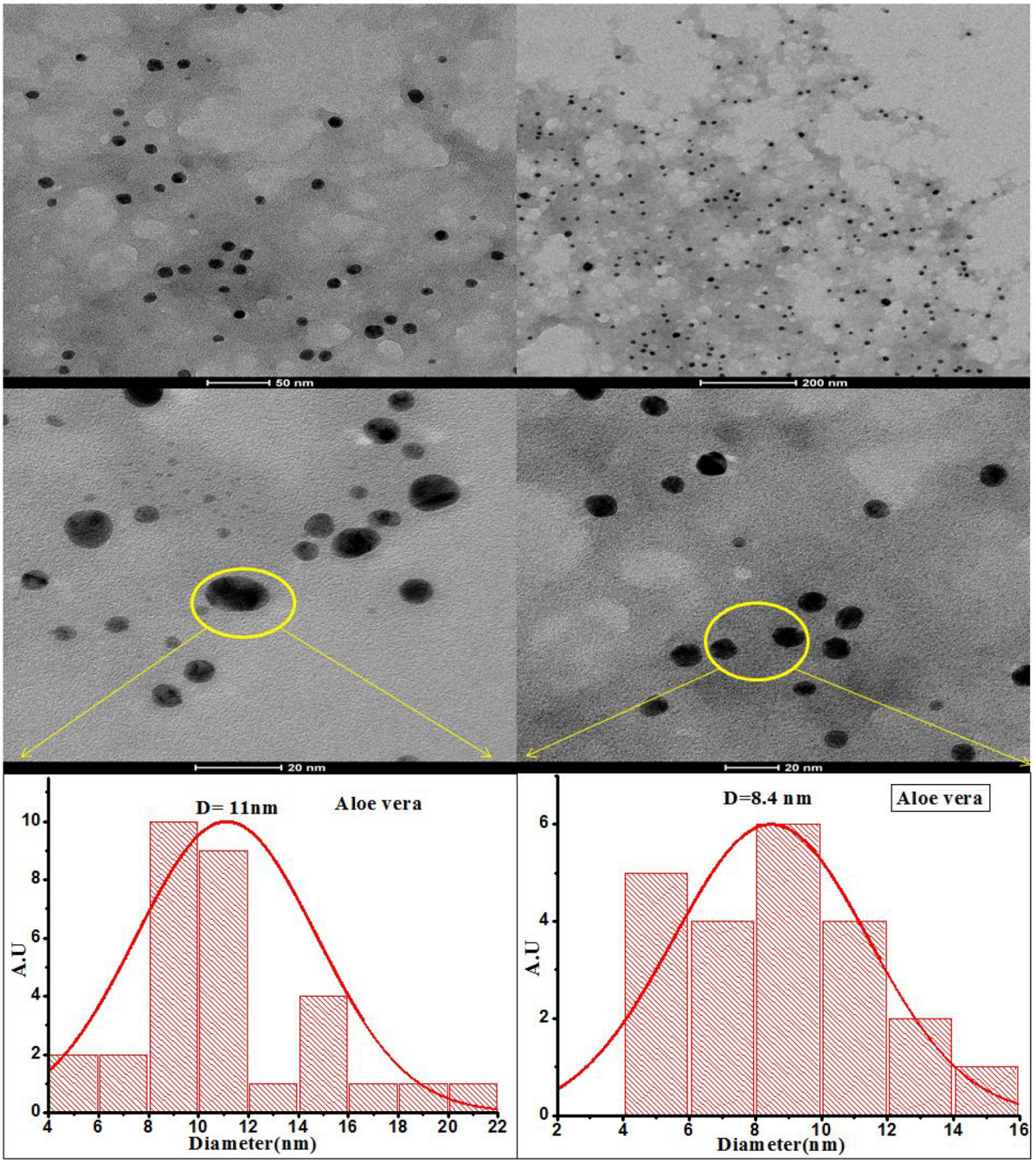

Figure 5. TEM images and particle distribution histogram of *Aloe vera*-mediated AgNPs.

the azo linkage in the presence of sodium borohydride and provoke free amino group hydrazine derivative, low molecular compounds,[48,49] as demonstrated in Scheme 1.

The percent reduction of the reaction was evaluated using Equation 1 from their UV−visible spectra. Figure 7c displays that our nanoparticles have a good MO reduction, with a 57% reduction in 14 min. As a result, the reduction/degradation of MO by our biogenic AgNPs is relatively high, especially when compared to a recent study that found that ∼80% of MO degradation takes 45 min utilizing *Mussaenda erythrophylla*-mediated silver nanoparticles.[48] This proposes that our catalyst has an exceptional catalytic reduction ability.

The reduction/degradation of MO dye by sodium borohydride follows the *pseudo-first-order* reaction and was calculated from the linear plot of $\ln(A_t/A_0)$ versus reduction time using Equation 3.

$$\ln \frac{C_t}{C_0} = -kK_t = -k_{app}t$$

$$\text{OR} \quad \ln \frac{A_t}{A_0} = -kK_t = -k_{app}t \tag{3}$$

Thus, the *pseudo-first-order* (k_{app}) calculated for MO dye from the slope for AgNPs at the average temperature was 6.03 × 10^{-4} s^{-1} (Figure 7d).

3.8. Hydrogenation of PNP. *para*-Nitrophenol is a hazardous organic pollutant impervious to biodegradation and is, thus, persistent. Researchers are concentrating their

https://doi.org/10.1021/acsomega.1c07365
ACS Omega 2022, 7, 14723−14734

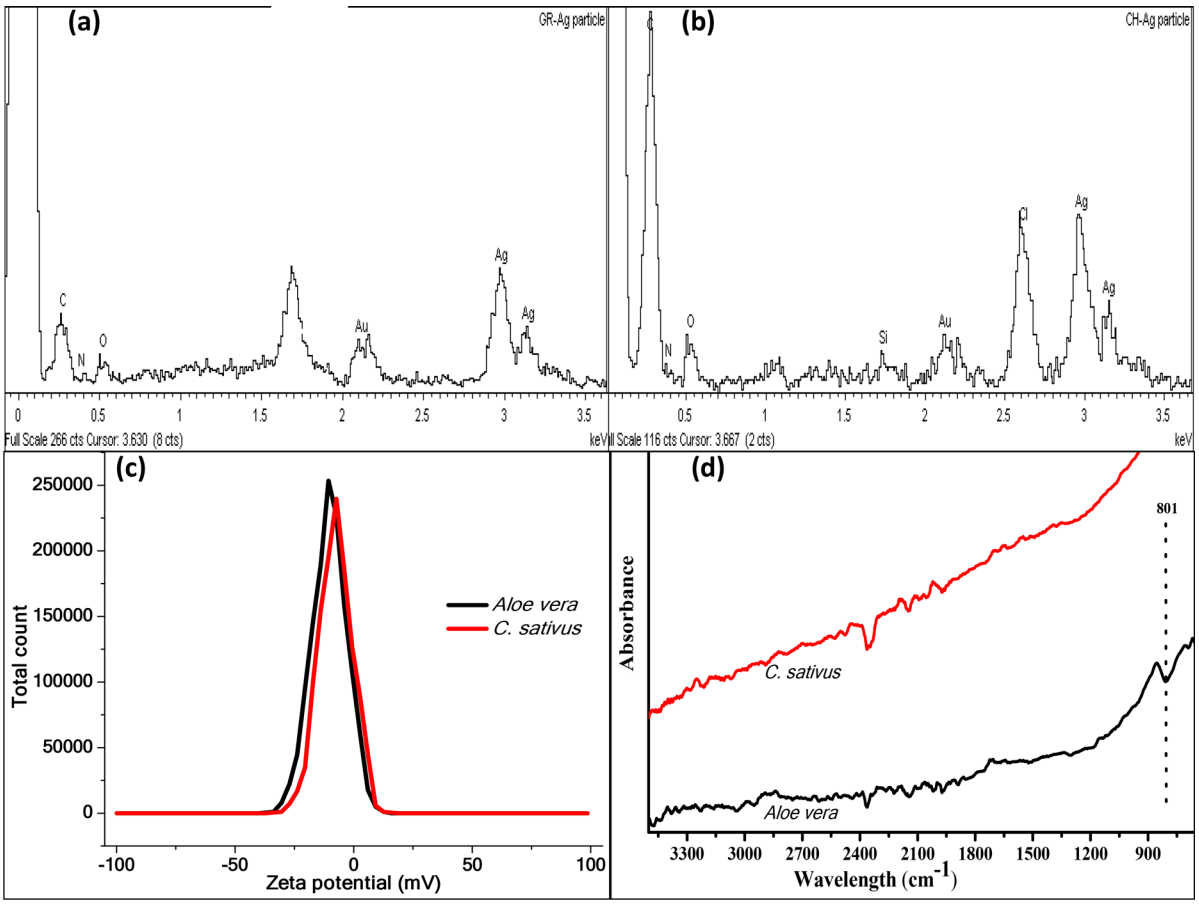

Figure 6. EDX investigation of (a) *C. sativus*- and (b) *Aloe vera*-mediated AgNPs. (c) Zeta potential value of *C. sativus*- and *Aloe vera*-mediated AgNPs. (d) FTIR spectra of *C. sativus*- and *Aloe vera*-mediated AgNPs.

efforts on reducing and removing this pollutant from the environment. Note that the sodium borohydride-mediated PNP reduction has been used as a model reaction to investigate the catalytic activity of the catalyst toward nitroaromatic chemicals because this reaction is simple to measure.[50]

Biogenic AgNPs in the presence of $NaBH_4$ could catalytically convert the hazardous PNP to the corresponding PAP. When 0.5 mL of 0.1 M $NaBH_4$ was added to the cuvette containing 2.5 mL of 0.1 mM PNP solution, the light yellow color of PNP turned bright yellow, and the wavelength shifted from 321 to 401 nm under alkaline conditions.[51] The addition of $NaBH_4$ altered the pH of the solution mixture due to the production of *para*-nitrophenolate ions that emerged at 401 nm. The reaction mixture containing PNP without AgNPs was stable for up to 30 min using a time-dependent UV−visible spectrophotometer, with higher absorbance at 401 nm. PAP was synthesized with the addition of 10 mg of biogenic AgNPs, which worked as a catalyst, converting PNP to PAP. The solution turns colorless when the reaction is complete, indicating that PNP has been entirely reduced to PAP. The new peak for PAP appeared at 301 nm after 13 min. The catalytic reduction of PNP to PAP results in the loss of the 401 nm peak and a new peak at 301 nm.[25,52,53]

It was previously reported that only $NaBH_4$ cannot reduce/hydrogenate PNP.[52] As earlier verified that at the normal condition, the hydrogenation of PNP (E_1/4 _0.76 V) is possible thermodynamically because, in an aqueous medium, borohydride ions (BH_4^-) (E_1/4 _1.33 V) act as a reductant. But kinetically, in the absence of a specific catalyst, the hydrogenation of the PNP to PAP is unfavorable and incredibly difficult to occur. This is due to the kinetic barrier of borohydride ions (BH_4^-) and phenolate ions ($C_6H_4NO_3^-$) that repel mutually each other.[54] For a quick electron transfer from an electron donor ($NaBH_4$) to an electron acceptor (PNP) to catalytically reduce PNP, small AgNPs can supply more catalytic sites than large AgNPs.[55] The plausible hydrogenation mechanism of the PNP to PAP by a AgNPs catalyst in the presence of sodium borohydride is demonstrated in Scheme 2.

Thus, the hydrogenation process needed active catalysts like AgNPs to catalyze this process. Equation 1 was used to compute the percent reduction of PNP by AgNPs catalyst. The AgNPs catalyst (Figure 7c) reduces PNP by 98.23% in 13 min. The apparent rate constant (k_{app}) of the *pseudo-first-order* reaction, calculated from the plot of $\ln(A_t/A_0)$ versus time of reduction in seconds using Equation 2 at normal temperature, was 1.51×10^{-3} s^{-1}.

3.9. Antibacterial Activity. The agar well diffusion method was used to assess in vitro antibacterial activity on nutrient agar. This approach relies on antimicrobial component diffusion from the reservoir hole to the surrounding inoculated nutrient agar medium, inhibiting microbe growth as a zone around the hole. In a 1 mL saline solution, new cultures of *K. pneumonia*, *Enterobacter*, *S. aureus*, and *S. pneumonia* bacteria were mixed with a wire loop. Inoculums of 10^{-1} were generated by mixing 1 mL of bacterial-containing saline solution with another saline solution. A sterile spreader was

https://doi.org/10.1021/acsomega.1c07365
ACS Omega 2022, 7, 14723−14734

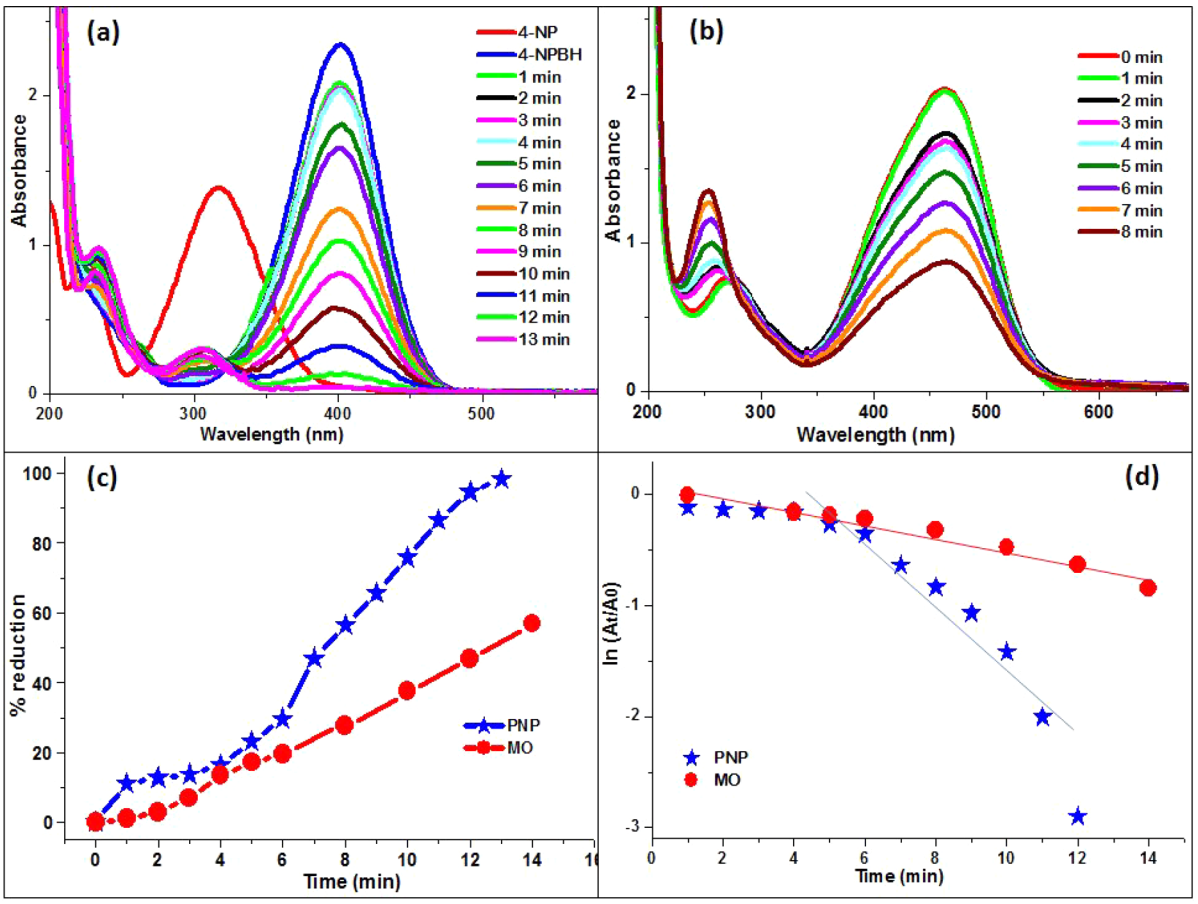

Figure 7. Catalytic reduction ability of *Aloe vera*-mediated AgNPs against (a) PNP by $NaBH_4$ and (b) MO by $NaBH_4$. (c) Percent reduction. (d) Plot of ln A_t/A_o vs time.

Scheme 1. Plausible Reduction Mechanism of MO by AgNPs Catalyst in the Presence of Sodium Borohydride

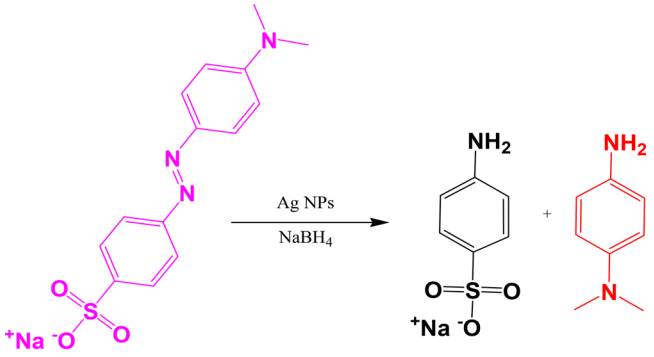

Scheme 2. Plausible Hydrogenation Mechanism of PNP to PAP by AgNPs Catalyst in the Presence of Sodium Borohydride

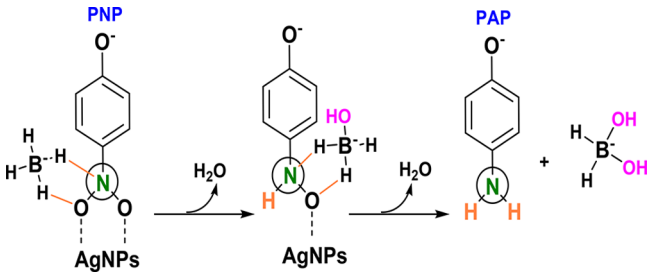

used to disperse a 100 μL bacterial solution on the medium surface, and a cork borer was employed to punch holes. The diameter of the holes punched out in the agar medium was 6 mm. By micropipette, 25, 50, 75, and 100 μL of the AgNPs were poured into wells, while 50 μL of clarithromycin served as a control. For the effective diffusion of the test and standard, the plates were maintained in the refrigerator for 2 h at 2−8 °C. They were then cultured for 24 h at 37 °C in a bacterial strain incubator. The widths of the extract-induced inhibitory zones were compared to those produced by clarithromycin (30 mg/mL), a commercial control antibiotic. The inhibition zone was measured in millimeters.

The in vitro antibacterial activity of *Aloe vera* and *Cucumis sativus* AgNPs was tested against the bacterial activity. As shown in the paper, the zone of inhibition extended from 10 ± 0.02 to 22 ± 0.02 (Table 1). 25, 50, 75, and 100 μL of *Aloe vera* and *Cucumis sativus*-mediated AgNPs were employed. The zone of inhibition against *K. pneumoniae* was 11 ± 0.02 mm at a concentration of 25 μL, 15 mm at a concentration of 50 μL, 18 mm at a concentration of 75 μL, and 21 mm at a concentration of 100 μL (Figure 8). *Enterobacter*, *S. aureus*, and *S. pneumoniae* are three types of bacteria. The maximum activity of the conventional antibiotic clarithromycin against *S. pneumoniae* was 25 mm at a concentration of 50 μL. The AgNPs of *Aloe vera* and *Cucumis sativus* had good anti-*K.*

https://doi.org/10.1021/acsomega.1c07365
ACS Omega 2022, 7, 14723−14734

Table 1. Zone of Inhibition of *Aloe vera* and *Cucumis sativus*-Mediated AgNPs against Bacteria

Sr. No.	organisms (bacteria)	concentration of AgNPs (Av+Cs)				control (Clarithromycin)
		25 μL	50 μL	75 μL	100 μL	50 μL
1	*K. pneumoniae*	11 ± 0.02	15 ± 0.02	18 ± 0.02	21 ± 0.02	23 ± 0.02
2	*Enterobacter*	12 ± 0.02	14 ± 0.02	17 ± 0.02	22 ± 0.02	24 ± 0.02
3	*S. aureus*	10 ± 0.02	14 ± 0.02	19 ± 0.02	21 ± 0.02	24 ± 0.02
4	*S. pneumoniae*	11 ± 0.02	16 ± 0.02	18 ± 0.02	22 ± 0.02	25 ± 0.02

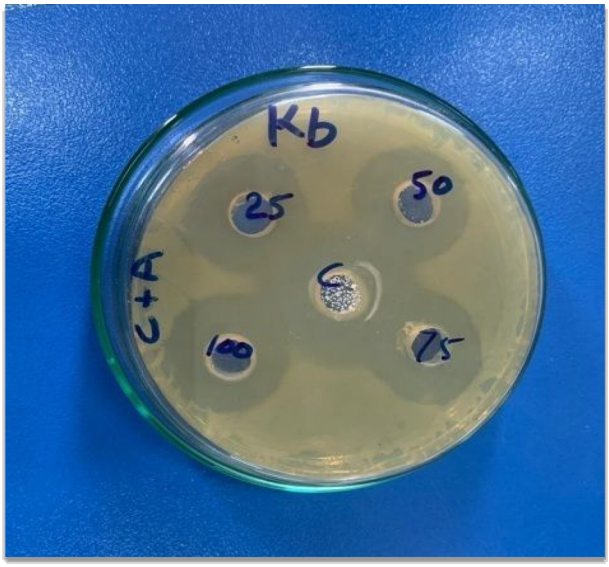

Figure 8. Zone of inhibition of AgNPs against *K. pneumonia* (Photograph courtesy of Muhammad Riaz. Copyright 2022).

pneumoniae action. The antimicrobial assay result is depicted in Figure 9. As shown in the data, the diameter of the inhibitory zone for Gram-negative bacteria is more significant than that of Gram-positive bacteria.

This could be because their cell walls' makeup is different.[56] Gram-negative bacteria have a single-layer peptidoglycan cell barrier, but Gram-positive bacteria have a multilayer peptidoglycan cell wall, making it stiffer for penetration.[57] Previous research claims that silver nanoparticles emit Ag^+ ions when they come close to bacterial cells, resulting in antibiotic action.[58] Because silver cations have a slight negative charge, they are drawn to the bacterial cell wall. When Ag^+ ions are electrostatically attracted to the bacterial cell wall, they migrate toward it and attach to it. As a result, the cell wall composition changes rapidly, influencing the permeability of the cell wall. Cellular transport is further harmed, and cells die.[59] *Aloe vera* and *Cucumis sativus*-mediated AgNPs may have antibacterial action against bacteria that are known to be a primary cause of skin infection and could be helpful in treating the exact in vivo disease pathology.

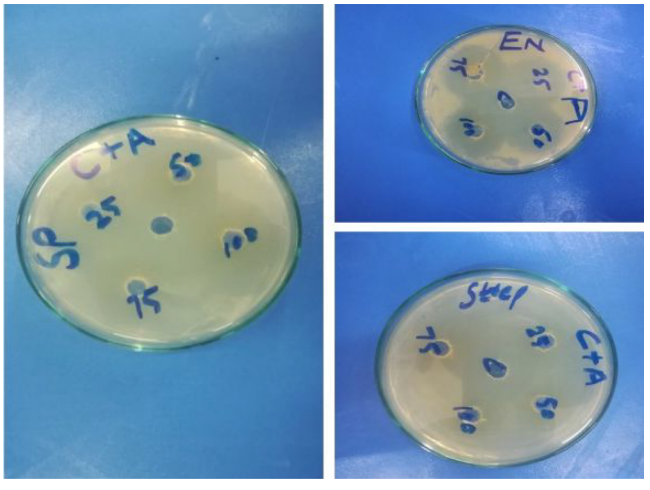

Figure 9. Zone of inhibition of AgNPs against *Enterobacter*, *S. aureus* (Staph), and *S. pneumonia* (Photograph courtesy of Muhammad Riaz. Copyright 2022).

4. CONCLUSION

The present study reported a green approach for the synthesis of AgNPs using a *C. sativus* and *Aloe vera* aqueous extract. The procedure is rapid, easy, cost-effective, and eco-friendly and did not require any solvents or reagents except water. Green synthesis approaches are becoming increasingly popular as a one-step, cost-effective, and environmentally friendly alternative to traditional chemical and physical syntheses. In the current study, additional strength has been given for the preparation using *Aloe vera* and *C. sativus*, as it is one of the important sources for the synthesis of spherical as well as face centered-cubic shaped AgNPs.

UV−visible spectroscopy revealed an SPR band at 405 nm, which confirms the formation of AgNPs. TEM confirmed the spherical shape AgNPs with an average diameter of ∼8.4 ± 2 nm. XRD confirms the crystalline nature and face-centered cubic structure of AgNPs. FT-IR spectra confirmed that biomolecules of *Aloe vera* and *C. sativus* were responsible for the reduction and capping of AgNPs. A catalytic investigation of biogenic silver nanoparticles effectively reduces methyl orange dye and *para*-nitrophenol. As evidenced by catalytic degradation and antibacterial activities, AgNPs were more active than the precursors.

AUTHOR INFORMATION

Corresponding Authors

Muhammad Ismail − *Department of Chemistry, Kohat University of Science & Technology, Kohat 26000 Khyber Pakhtunkhwa, Pakistan;* orcid.org/0000-0002-8185-0511; Email: ismailkust@yahoo.com

Jeongwon Park − *School of Electrical Engineering and Computer Science, University of Ottawa, Ottawa K1N 6N5 Ontario, Canada; Department of Electrical and Biomedical Engineering, University of Nevada, Reno 89557 Nevada, United States;* orcid.org/0000-0003-4988-302X; Email: jpark2@uottawa.ca

Authors

Muhammad Riaz − *Department of Biological Sciences, International Islamic University Islamabad, Islamabad 44000, Pakistan; School of Electrical Engineering and Computer Science, University of Ottawa, Ottawa K1N 6N5 Ontario, Canada*

https://doi.org/10.1021/acsomega.1c07365
ACS Omega 2022, 7, 14723−14734

Uzma Sharafat − *Institute of Chemical Sciences, University of Swat, Swat 19200 Khyber Pakhtunkhwa, Pakistan*
Nafeesa Zahid − *Department of Botany, Mirpur University of Science and Technology, Mirpur 10250 Azad Kashmir, Pakistan*
Bashir Ahmad − *Department of Biological Sciences, International Islamic University Islamabad, Islamabad 44000, Pakistan*
Neelum Rashid − *Department of Botany, Mirpur University of Science and Technology, Mirpur 10250 Azad Kashmir, Pakistan*
Muhammad Fahim − *Department of Biological Sciences, International Islamic University Islamabad, Islamabad 44000, Pakistan*
Muhammad Imran − *Department of Biological Sciences, International Islamic University Islamabad, Islamabad 44000, Pakistan*
Aisha Tabassum − *Department of Biochemistry, University of Sialkot, Sialkot 51040, Pakistan*

Complete contact information is available at:
https://pubs.acs.org/10.1021/acsomega.1c07365

Notes

The authors declare no competing financial interest.
Data availability. The authors confirm that the data supporting the findings of this study are available within the article.

■ ACKNOWLEDGMENTS

The authors are highly grateful for the Department of Biological Sciences, Faculty of Basic and Applied Sciences, International Islamic University, H-10, Islamabad, and the Department of Chemistry Kohat University of Science and Technology, Kohat-2600, Pakistan. Part of this study was funded under a project conducted at the University of Ottawa, Ontario, Canada.

■ REFERENCES

(1) Ismail, M.; Gul, S.; Khan, M. A.; Khan, M. Plant Mediated Green Synthesis of Anti-Microbial Silver Nanoparticles—A Review on Recent Trends. *Reviews Nanosci Nanotechnol* **2016**, *5* (2), 119−135.
(2) Huang, Y.; Xu, H.; Yang, H.; Lin, Y.; Liu, H.; Tong, Y. Efficient charges separation using advanced BiOI-based hollow spheres decorated with palladium and manganese dioxide nanoparticles. *ACS Sustainable Chem. Eng.* **2018**, *6* (2), 2751−2757.
(3) Ismail, M.; Khan, M. I.; Akhtar, K.; Khan, M. A.; Asiri, A. M.; Khan, S. B. Biosynthesis of silver nanoparticles: A colorimetric optical sensor for detection of hexavalent chromium and ammonia in aqueous solution. *Physica E:* **2018**, *103*, 367−376.
(4) Albukhari, S. M.; Ismail, M.; Akhtar, K.; Danish, E. Y. Catalytic reduction of nitrophenols and dyes using silver nanoparticles @ cellulose polymer paper for the resolution of waste water treatment challenges. *Colloids Surf. A:* **2019**, *577*, 548−561.
(5) Ismail, M.; Gul, S.; Khan, M.; Khan, M. A.; Asiri, A. M.; Khan, S. B. Medicago polymorpha-mediated antibacterial silver nanoparticles in the reduction of methyl orange. *Green Process. Synth* **2019**, *8* (1), 118−127.
(6) Syed, A.; Saraswati, S.; Kundu, G. C.; Ahmad, A. Biological synthesis of silver nanoparticles using the fungus Humicola sp. and evaluation of their cytoxicity using normal and cancer cell lines. *Spectrochimica Acta Part A:* **2013**, *114*, 144−147.
(7) Seshadri, S.; Prakash, A.; Kowshik, M. Biosynthesis of silver nanoparticles by marine bacterium, Idiomarina sp. PR58−8. *Bulletin Mater. Sci.* **2012**, *35* (7), 1201−1205.
(8) Gul, S.; Ismail, M.; Khan, M. I.; Khan, S. B.; Asiri, A. M.; Rahman, I. U.; Khan, M. A.; Kamboh, M. A. Novel synthesis of silver nanoparticles using melon aqueous extract and evaluation of their feeding deterrent activity against housefly Musca domestica. *Asian Pacific J. Trop Dis* **2016**, *6* (4), 311−316.
(9) Riaz, M.; Mutreja, V.; Sareen, S.; Ahmad, B.; Faheem, M.; Zahid, N.; Jabbour, G.; Park, J. Exceptional antibacterial and cytotoxic potency of monodisperse greener AgNPs prepared under optimized pH and temperature. *Sci. Rep.* **2021**, *11* (1), 1−11.
(10) Li, S.; Shen, Y.; Xie, A.; Yu, X.; Qiu, L.; Zhang, L.; Zhang, Q. Green synthesis of silver nanoparticles using Capsicum annuum L. extract. *Green Chem.* **2007**, *9* (8), 852−858.
(11) Medda, S.; Hajra, A.; Dey, U.; Bose, P.; Mondal, N. K. Biosynthesis of silver nanoparticles from Aloe vera leaf extract and antifungal activity against Rhizopus sp. and Aspergillus sp. *Applied Nanosci* **2015**, *5* (7), 875−880.
(12) Rajeshkumar, S.; Bharath, L. Mechanism of plant-mediated synthesis of silver nanoparticles−a review on biomolecules involved, characterisation and antibacterial activity. *Chemico-biological Interactions* **2017**, *273*, 219−227.
(13) Sathishkumar, M.; Sneha, K.; Won, S.; Cho, C.-W.; Kim, S.; Yun, Y.-S. Cinnamon zeylanicum bark extract and powder mediated green synthesis of nano-crystalline silver particles and its bactericidal activity. *Colloids Surf. B:* **2009**, *73* (2), 332−338.
(14) Ahmed, S.; Ahmad, M.; Swami, B. L.; Ikram, S. A review on plants extract mediated synthesis of silver nanoparticles for antimicrobial applications: a green expertise. *J. Adv. Res.* **2016**, *7* (1), 17−28.
(15) Safajou, H.; Ghanbari, M.; Amiri, O.; Khojasteh, H.; Namvar, F.; Zinatloo-Ajabshir, S.; Salavati-Niasari, M. Green synthesis and characterization of RGO/Cu nanocomposites as photocatalytic degradation of organic pollutants in waste-water. *Int. J. Hydro Energy* **2021**, *46* (39), 20534−20546.
(16) Karami, M.; Ghanbari, M.; Alshamsi, H. A.; Rashki, S.; Salavati-Niasari, M. Facile fabrication of Tl 4 HgI 6 nanostructures as novel antibacterial and antibiofilm agents and photocatalysts in the degradation of organic pollutants. *Inorg. Chem. Frontiers* **2021**, *8* (10), 2442−2460.
(17) Spain, J. C. Biodegradation of Nitroaromatic Compounds. *Annu. Rev. Microbiol.* **1995**, *49* (1), 523−555.
(18) Mortazavi-Derazkola, S.; Zinatloo-Ajabshir, S.; Salavati-Niasari, M. Novel simple solvent-less preparation, characterization and degradation of the cationic dye over holmium oxide ceramic nanostructures. *Ceram. Int.* **2015**, *41* (8), 9593−9601.
(19) Huang, Y.; Lu, Y.; Lin, Y.; Mao, Y.; Ouyang, G.; Liu, H.; Zhang, S.; Tong, Y. Cerium-based hybrid nanorods for synergetic photo-thermocatalytic degradation of organic pollutants. *J. Mater. Chem. A* **2018**, *6* (48), 24740−24747.
(20) Shen, J.; He, R.; Wang, L.; Zhang, J.; Zuo, Y.; Li, Y.; Sun, X.; Li, J.; Han, W. Biodegradation kinetics of picric acid by Rhodococcus sp.NJUST16 in batch reactors. *J. Hazard. Mater.* **2009**, *167* (1), 193−198.
(21) Michałowicz, J.; Duda, W. Phenols−Sources and Toxicity *Polish J. Environ. Studies* **2007**, *16* (3).
(22) Chen, H. Recent advances in azo dye degrading enzyme research. *Current Protein and Peptide Science* **2006**, *7* (2), 101−111.
(23) Cheng, N.; Tian, J.; Liu, Q.; Ge, C.; Qusti, A. H.; Asiri, A. M.; Al-Youbi, A. O.; Sun, X. Au-nanoparticle-loaded graphitic carbon nitride nanosheets: green photocatalytic synthesis and application toward the degradation of organic pollutants. *ACS applied mater. interf* **2013**, *5* (15), 6815−6819.
(24) Ismail, M.; Khan, M. I.; Khan, S. B.; Khan, M. A.; Akhtar, K.; Asiri, A. M. Green synthesis of plant supported CuAg and CuNi bimetallic nanoparticles in the reduction of nitrophenols and organic dyes for water treatment. *J. Mol. Liq.* **2018**, *260*, 78−91.
(25) Ismail, M.; Khan, M.; Khan, S. B.; Akhtar, K.; Khan, M. A.; Asiri, A. M. Catalytic reduction of picric acid, nitrophenols and organic azo dyes via green synthesized plant supported Ag nanoparticles. *J. Mol. Liq.* **2018**, *268*, 87−101.
(26) Li, Y.; Liu, K.; Zhang, J.; Yang, J.; Huang, Y.; Tong, Y. Engineering the band-edge of Fe2O3/ZnO nanoplates via separate

dual cation incorporation for efficient photocatalytic performance. *Indus. Engin. Chem. Res.* **2020**, *59* (42), 18865−18872.
(27) Huang, Y.; Guo, Z.; Liu, H.; Zhang, S.; Wang, P.; Lu, J.; Tong, Y. Heterojunction architecture of N-doped WO_3 nanobundles with Ce_2S_3 nanodots hybridized on a carbon textile enables a highly efficient flexible photocatalyst. *Adv. Functional Mater.* **2019**, *29* (45), 1903490.
(28) Riaz, M.; Ismail, M.; Ahmad, B.; Zahid, N.; Jabbour, G.; Khan, M. S.; Mutreja, V.; Sareen, S.; Rafiq, A.; Faheem, M.; et al. Characterizations and analysis of the antioxidant, antimicrobial, and dye reduction ability of green synthesized silver nanoparticles. *Green Process. Synth* **2020**, *9* (1), 693−705.
(29) Abdallah, B. M.; Ali, E. M. Green synthesis of silver nanoparticles using the Lotus lalambensis aqueous leaf extract and their anti-candidal activity against oral candidiasis. *ACS omega* **2021**, *6* (12), 8151−8162.
(30) Hemlata; Meena, P. R.; Singh, A. P.; Tejavath, K. K. Biosynthesis of Silver Nanoparticles Using Cucumis prophetarum Aqueous Leaf Extract and Their Antibacterial and Antiproliferative Activity Against Cancer Cell Lines. *ACS Omega* **2020**, *5* (10), 5520−5528.
(31) Ismail, M.; Khan, M. I.; Akhtar, K.; Seo, J.; Khan, M. A.; Asiri, A. M.; Khan, S. B. Phytosynthesis of silver nanoparticles; naked eye cellulose filter paper dual mechanism sensor for mercury ions and ammonia in aqueous solution. *J. Mater. Sci: Mater. in Electronics* **2019**, *30* (8), 7367−7383.
(32) Bilal, M.; Khan, S.; Ali, J.; Ismail, M.; Khan, M. I.; Asiri, A. M.; Khan, S. B. Biosynthesized silver supported catalysts for disinfection of Escherichia coli and organic pollutant from drinking water. *J. Mol. Liq.* **2019**, *281*, 295−306.
(33) Zheng, M.; Wang, Z.-s.; Zhu, Y.-w. Preparation of silver nanoparticle via active template under ultrasonic. *Transactions of Nonferrous Metals Society of China* **2006**, *16* (6), 1348−1352.
(34) Khan, A.; Asiri, A. M.; Rub, M. A.; Azum, N.; Khan, A. A. P.; Khan, S. B.; Rahman, M. M.; Khan, I. Synthesis, characterization of silver nanoparticle embedded polyaniline tungstophosphate-nano-composite cation exchanger and its application for heavy metal selective membrane. *Composites Part B: Engineering* **2013**, *45* (1), 1486−1492.
(35) Rizwana, H.; Alwhibi, M. S.; Aldarsone, H. A.; Awad, M. A.; Soliman, D. A.; Bhat, R. S. Green synthesis, characterization, and antimicrobial activity of silver nanoparticles prepared using Trigonella foenum-graecum L. leaves grown in Saudi Arabia. *Green Process. Synth* **2021**, *10* (1), 421−429.
(36) Tüzün, B. S.; Hohmann, J.; Kivcak, B. Green bio-inspired synthesis, characterization and activity of silver nanoparticle forms of Centaurea virgata Lam. and the isolated flavonoid eupatorin. *Green Process. Synth* **2018**, *7* (4), 372−379.
(37) Heydari, R.; Rashidipour, M. Green Synthesis of Silver Nanoparticles Using Extract of Oak Fruit Hull (Jaft): Synthesis and In Vitro Cytotoxic Effect on MCF-7 Cells. *International J. Breast Cancer* **2015**, *2015*, 846743.
(38) Saha, P.; Mahiuddin, M.; Islam, A. B. M. N.; Ochiai, B. Biogenic Synthesis and Catalytic Efficacy of Silver Nanoparticles Based on Peel Extracts of Citrus macroptera Fruit. *ACS Omega* **2021**, *6* (28), 18260−18268.
(39) Rolim, W. R.; Pelegrino, M. T.; de Araújo Lima, B.; Ferraz, L. S.; Costa, F. N.; Bernardes, J. S.; Rodigues, T.; Brocchi, M.; Seabra, A. B. Green tea extract mediated biogenic synthesis of silver nanoparticles: Characterization, cytotoxicity evaluation and antibacterial activity. *Appl. Surf. Sci.* **2019**, *463*, 66−74.
(40) Roy, K.; Sarkar, C.; Ghosh, C. Plant-mediated synthesis of silver nanoparticles using parsley (Petroselinum crispum) leaf extract: spectral analysis of the particles and antibacterial study. *Applied Nanosci* **2015**, *5* (8), 945−951.
(41) Ismail, M.; Khan, M.; Khan, S. A.; Qayum, M.; Khan, M. A.; Anwar, Y.; Akhtar, K.; Asiri, A. M.; Khan, S. B. Green synthesis of antibacterial bimetallic Ag−Cu nanoparticles for catalytic reduction of persistent organic pollutants. *J. Mater. Sci: Mater. Electronics* **2018**, *29* (24), 20840−20855.
(42) Khan, S. B.; Ismail, M.; Bakhsh, E. M.; Asiri, A. M. Design of simple and efficient metal nanoparticles templated on ZnO-chitosan coated textile cotton towards the catalytic reduction of organic pollutants. *Journal of Industrial Textiles* **2020**, DOI: 10.1177/1528083720931481.
(43) Ramamurthy, C.; Padma, M.; Mareeswaran, R.; Suyavaran, A.; Kumar, M. S.; Premkumar, K.; Thirunavukkarasu, C.; et al. The extra cellular synthesis of gold and silver nanoparticles and their free radical scavenging and antibacterial properties. *Colloids Surf., B* **2013**, *102*, 808−815.
(44) Munagapati, V. S.; Yarramuthi, V.; Kim, D.-S. Methyl orange removal from aqueous solution using goethite, chitosan beads and goethite impregnated with chitosan beads. *J. Mol. Liq.* **2017**, *240*, 329−339.
(45) Ismail, M.; Akhtar, K.; Khan, M.; Kamal, T.; Khan, M. A.; M Asiri, A.; Seo, J.; Khan, S. B. Pollution, Toxicity and Carcinogenicity of Organic Dyes and their Catalytic Bio-Remediation. *Current pharmaceutical design* **2019**, *25* (34), 3645−3663.
(46) Ali, F.; Khan, S. B.; Kamal, T.; Anwar, Y.; Alamry, K. A.; Asiri, A. M. Anti-bacterial chitosan/zinc phthalocyanine fibers supported metallic and bimetallic nanoparticles for the removal of organic pollutants. *Carbohydr. Polym.* **2017**, *173*, 676−689.
(47) Khan, M. M.; Lee, J.; Cho, M. H. Au@ TiO 2 nanocomposites for the catalytic degradation of methyl orange and methylene blue: an electron relay effect. *Journal of Industrial and Engineering Chemistry* **2014**, *20* (4), 1584−1590.
(48) Varadavenkatesan, T.; Selvaraj, R.; Vinayagam, R. Phyto-synthesis of silver nanoparticles from Mussaenda erythrophylla leaf extract and their application in catalytic degradation of methyl orange dye. *J. Mol. Liq.* **2016**, *221*, 1063−1070.
(49) Al-hamoud, K.; Shaik, M. R.; Khan, M.; Alkhathlan, H. Z.; Adil, S. F.; Kuniyil, M.; Assal, M. E.; Al-Warthan, A.; Siddiqui, M. R. H.; Tahir, M. N.; et al. Pulicaria undulata Extract-Mediated Eco-Friendly Preparation of TiO2 Nanoparticles for Photocatalytic Degradation of Methylene Blue and Methyl Orange. *ACS Omega* **2022**, *7* (6), 4812−4820.
(50) You, J. G.; Jin, D. Y.; Tseng, W. B.; Tseng, W. L.; Lin, P. C. Gold (I)-Thiolate Oligomers for Catalytic Hydrogenation of Nitroaromatics in Aqueous and Organic Medium. *ChemCatChem.* **2020**, *12* (18), 4558−4567.
(51) Cao, H.-L.; Liu, C.; Cai, F.-Y.; Qiao, X.-X.; Dichiara, A. B.; Tian, C.; Lü, J. In situ immobilization of ultra-fine Ag NPs onto magnetic Ag@RF@Fe3O4 core-satellite nanocomposites for the rapid catalytic reduction of nitrophenols. *Water Res.* **2020**, *179*, 115882.
(52) Ismail, M.; Khan, M. I.; Khan, M. A.; Akhtar, K.; Asiri, A. M.; Khan, S. B. Plant-supported silver nanoparticles: Efficient, economically viable and easily recoverable catalyst for the reduction of organic pollutants. *Appl. Organomet. Chem.* **2019**, *33* (8), No. e4971.
(53) Shah, Z.; Gul, T.; Ali Khan, S.; Shaheen, K.; Anwar, Y.; Suo, H.; Ismail, M.; Alghamdi, K. M.; Salman, S. M. Synthesis of high surface area AgNPs from Dodonaea viscosa plant for the removal of pathogenic microbes and persistent organic pollutants. *Materials Science and Engineering: B* **2021**, *263*, 114770.
(54) Saha, S.; Pal, A.; Kundu, S.; Basu, S.; Pal, T. Photochemical green synthesis of calcium-alginate-stabilized Ag and Au nanoparticles and their catalytic application to 4-nitrophenol reduction. *Langmuir* **2010**, *26* (4), 2885−2893.
(55) Wang, N.; Wang, F.; Pan, F.; Yu, S.; Pan, D. Highly efficient silver catalyst supported by a spherical covalent organic framework for the continuous reduction of 4-nitrophenol. *ACS Appl. Mater. Interfaces* **2021**, *13* (2), 3209−3220.
(56) Wahab, S.; Khan, T.; Adil, M.; Khan, A. Mechanistic aspects of plant-based silver nanoparticles against multi-drug resistant bacteria. *Heliyon* **2021**, *7*, 1.
(57) Prakash, P.; Gnanaprakasam, P.; Emmanuel, R.; Arokiyaraj, S.; Saravanan, M. Green synthesis of silver nanoparticles from leaf extract of Mimusops elengi, Linn. for enhanced antibacterial activity against

https://doi.org/10.1021/acsomega.1c07365
ACS Omega 2022, 7, 14723−14734

multi drug resistant clinical isolates. *Colloids Surf., B* **2013**, *108*, 255−259.
(58) Vimbela, G. V.; Ngo, S. M.; Fraze, C.; Yang, L.; Stout, D. A. Antibacterial properties and toxicity from metallic nanomaterials. *International journal of nanomedicine* **2017**, *12*, 3941.
(59) Jung, W. K.; Koo, H. C.; Kim, K. W.; Shin, S.; Kim, S. H.; Park, Y. H. Antibacterial activity and mechanism of action of the silver ion in Staphylococcus aureus and Escherichia coli. *Appl. Environ. Microbiol.* **2008**, *74* (7), 2171−2178.

https://doi.org/10.1021/acsomega.1c07365
ACS Omega 2022, 7, 14723−14734